INTERNAL EAVES CONNECTIONS OF DOUBLE-BAY COLD-FORMED STEEL PORTAL FRAMES

B Tshuma and M Dundu

University of Johannesburg, Department of Civil Engineering Science,
P.O. Box 524, Auckland Park, 2006, South Africa;
E-mail: morgandundu@gmail.com

Abstract:

Double-bay or multi-bay portal frames of hot-rolled steel have been in existence since the development of the plastic analysis theory, and the behaviour of the eaves connections of these frames are well established. With the increasing use of cold-formed steel in portal frames, it is necessary to develop connecting structural systems that are favourable to these elements, and to understand the behaviour of these connections. The purpose of this investigation is to develop internal eaves connections of double-bay portal frames of cold-formed steel channels, with the main frames members connected back-to-back. In double-bay portal frames, the columns of two single-bay portal frames, positioned adjacent to each other, are replaced by one internal column. Two internal eaves connections were developed and investigated, and are referred in this paper as Eaves Connection Type 1 (ECT-1) and Eaves Connection Type 2 (ECT-2). Tests were then performed to determine the capacity and failure mechanism of these connections, including the members forming these connections. Although the failure mechanisms included local buckling of the compression zone of the web and flange of the channels, and bolt-bearing deformations, all frames finally failed by local buckling of the web and flange of the channels. The moment-curvature graphs show that enough plasticity could not be achieved in both connections.

Keywords: Double-bay portal frames, cold-formed channels, eaves connections, local buckling, bearing deformations, joint stiffness.

1.0 Introduction

It has been proven in previous work that single cold-formed steel sections can be used as main structural elements in the construction of single portal frames, however, the challenge has always been to find the effective and economic way to connect the sections since the structural performance of a portal frame is mainly dependent on the structural performance of its connections. Baigent and Hancock [1] tested seven pitched-roof frames constructed from single cold-formed channels to destruction. The eaves joint construction used in the study consisted of two, 12 mm plates (a stiffening plate and a cover plate), cut to the correct angles and bolted rigidly to the webs of cold-formed channels using four, 19 mm diameter high tensile strength bolts at the end of each member. The configuration of the apex was of similar to the eaves joint and the joint at the base was a pin. Dundu [2], and Dundu and Kemp [3, 4] developed and performed an extensive research on lightweight portal frames. The column and rafter members of these portal frames were constructed from single channel sections, which were bolted, back-to-back at the eaves and apex joints, and connected to the foundation through angle cleats. An ingenious system was developed for connecting the purlin/girt to the rafter/column. A design approach of these portal frames is given in [5]. Further research work in this field has been performed on the use of angle cleats as base connections of single cold-formed steel portal

1

frames [6] and as restraints of single cold-formed channels against lateral torsional instability [7].

However, these studies were largely restricted to work that was done on single-bay portal frames formed from cold-formed steel channels. To extend this work, a decision was taken to develop internal eaves connections of double-bay portal frames. In double-bay portal frames, the columns of two single-bay portal frames, positioned adjacent to each other, are replaced by one internal column. The majority of double and/or multi-bay portal frames have slender internal columns because the moments at the eaves connection balance each other when the span of the portal frame is the same, and the portal frame is subjected to vertical downward loading, as shown in Figure 1. This allows the internal column to be designed for compression forces only. Although double-bay portal frames optimise the existence of two single portal frames positioned adjacent to each other, it is not easy to develop the structural configuration of the internal eaves connection. It should also be noted that although most behaviour and design characteristics of single-bay portal frames are similar to double-bay portal frames, the design of the internal eaves connections is different.
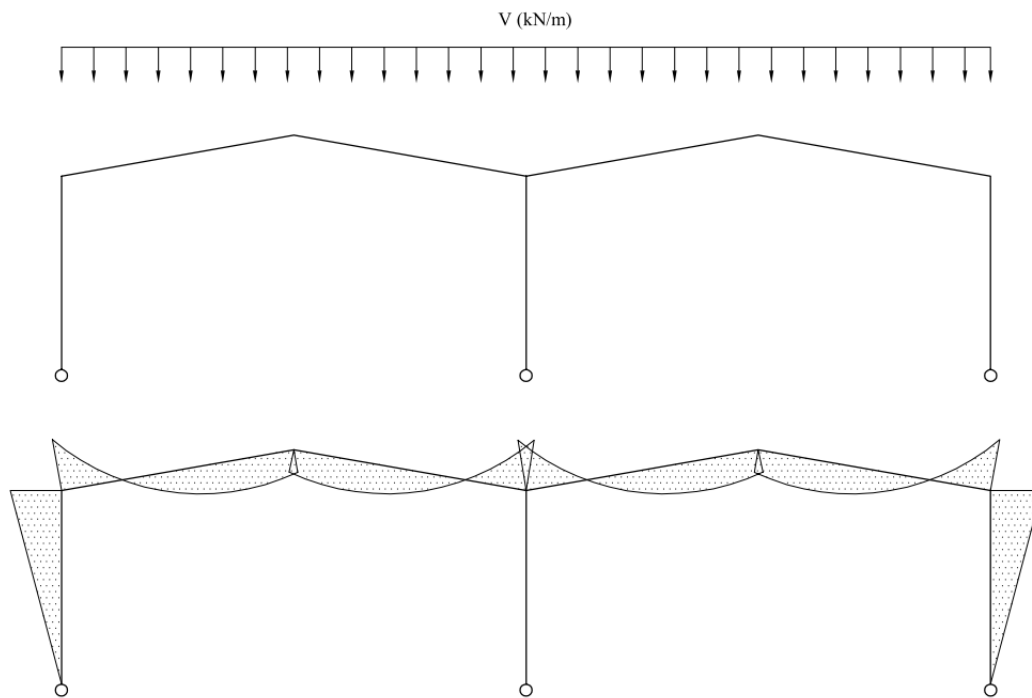

Figure 1: Bending moments in a double-bay portal frame under vertical downward loading

When horizontal loads are applied to the double-bay portal frame, as shown in Figure 2, only small shear forces and bending moments are resisted by the slender internal column(s), because the external columns provide a much larger portion of the stiffness. Due to these changes, the cost of a double or multi-bay portal frame is significantly cheaper than that of a two or multi-single-bay portal frame. The overall stability of a double or multi-bay portal frame is significantly higher than that of a two or multi-single-bay portal frame.
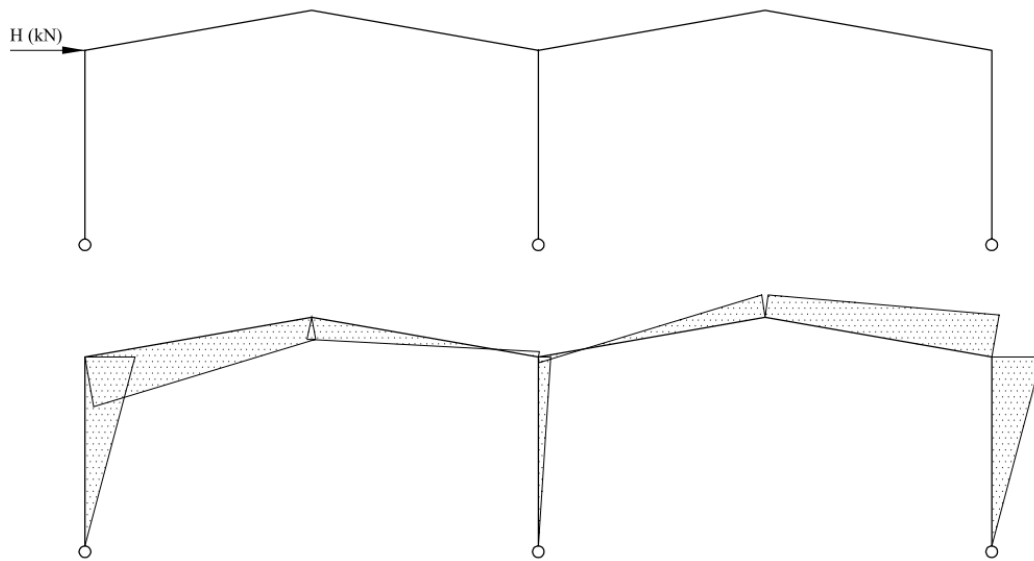
Figure 2: Bending moments in a double-bay portal frame under horizontal loading

As illustrated in Figure 3, the double-bay frame in Figure 2 can be treated as two sub-frames, each consisting of an external column and a two rafters. Since the majority of the stiffness is provided by the two external sub-frames in multi-bay frames, this model could analysed by hand. To understand the behaviour of internal eaves connections of lightweight, double-bay portal frame frames, made from cold-formed lipped channel sections, two eaves connection configurations were investigated, namely; Eaves Connection Type 1 (ECT-1) and Eaves Connection Type 2 (ECT-2).
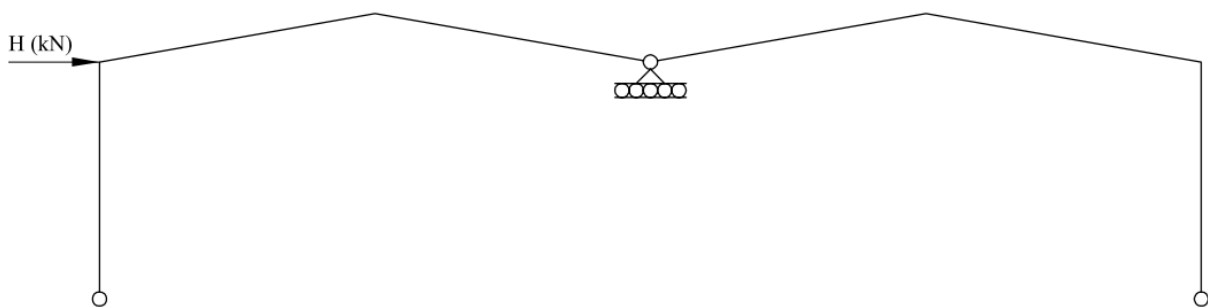

Figure 3: Sub-frames for a typical double-bay frame

In the first connection configuration (ECT-1), two rafters are connected, back-to-back, to the column, with one rafter connected to the column at a lower level than the other, as shown in Figure 4 [8]. This is a simply connection, as the column is connected to each rafter through 4 bolts only. In total, the connection uses 8, M20 bolts only. In this connection, no gusset plates, cleats or any secondary members are used. The joint uses less materials and labour. Since the rafters are connected at different levels in ECT-1, an unbalanced moment develops in the column. Although, this moment acts on a very short segment of the column, it should be taken into consideration when analysing and designing the connection. If the pitch of the double-bay portal is the same, to achieve equal bay clearances, the apex of the two bays must be at different heights (one higher than the other), and to achieve same apex heights, the bay clearances must be different (one less than the other), since rafters are connected at different levels. This structural arrangement may not be the best from an aesthetical point of view.

3

In the second eaves connection configuration (ECT-2), two rafters are connected back-to-back, to the column, at the same level through a hot-rolled steel gusset plate, as shown in Figure 5 [9]. This eliminates the unbalanced column moments in the ECT-1 connection configuration, allowing the central column to be designed for compression forces only, under vertical downward loading. The joint uses a total of 12, M20 bolts, 4 more that ECT-1 to cater for the gusset plate-to-column connection. From an aesthetical point of view, this joint configuration is neater than ECT-1, as rafters are connected at the same level. Unlike ECT-1, equal bays and apex heights of the bays can easily be achieved in this configuration. However, ECT-2 joints are cost and labour intensive, compared to ECT-1 joints, since they use more bolts and a hot-rolled steel gusset plate. In ECT-2, two thicknesses (6mm and 8mm) were chosen for the hot-rolled gusset plates. A theoretical analysis of the connection showed that a minimum gusset plate thickness of 6 mm would be able to resist the applied forces. A thicker gusset plate of 8mm was used in the research to increase the stiffness of the connection.
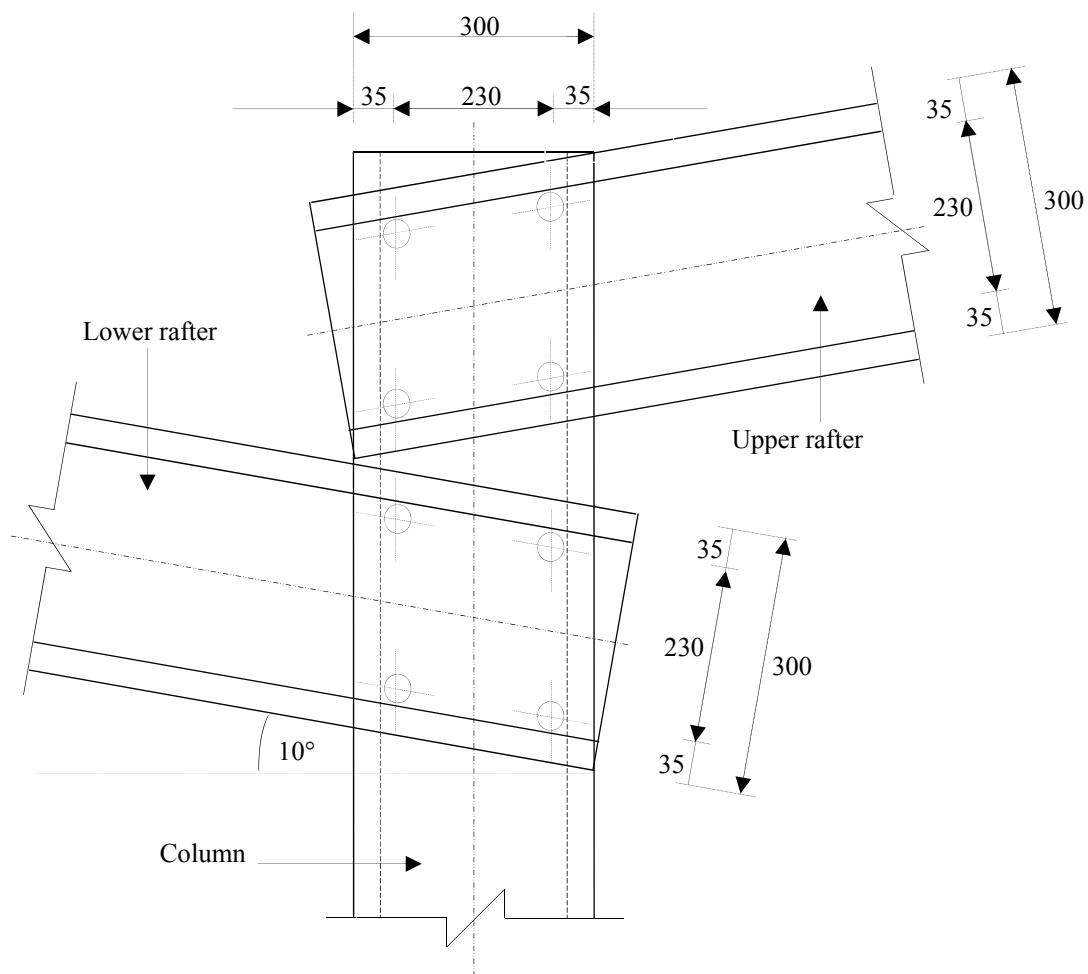

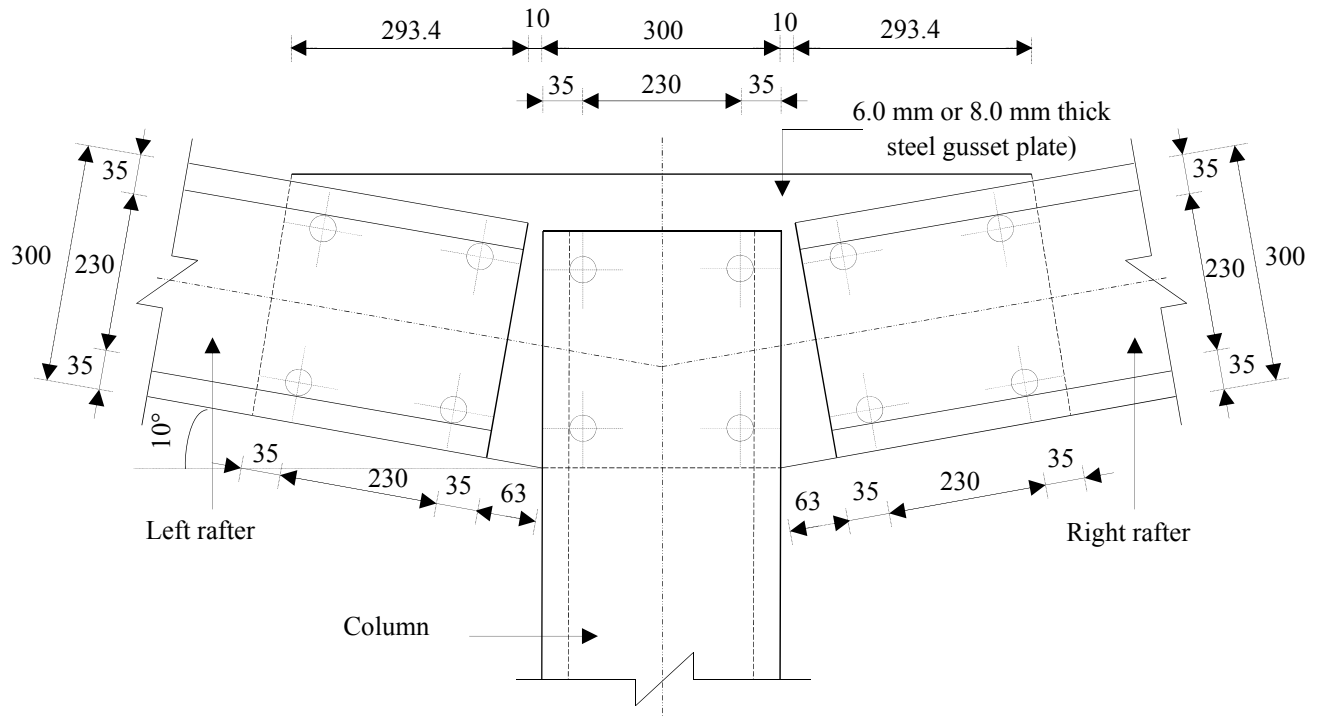Figure 4: Eaves Connection Type 1 (ECT-1)

4

Figure 5: Eaves Connection Type 2 (ECT-2)

In both connections (ECT-1 and ECT-2), the rafters were oriented in the opposite direction to the column, to take advantage of the counterbalancing moments and forces, developed as a result of the location of the shear centre of the connected channels [2, 3, 4]. To guard against premature failure of the connection and/or the rafters due to lateral-torsional buckling, the rafters were fully restrained. The objective of this investigation is to evaluate the structural performance of these eaves connections.

2.0 Material properties

The behaviour of a structural system depends mainly on their mechanical properties (yield strength, ultimate strength and ductility). It is therefore important to carry out tensile coupon tests in order to obtain their actual mechanical properties. The material properties of the cold-formed channels were obtained from thirty-three tensile coupon tests. Five coupons were cut from the web, three from the corners joining the web and another three from the flange of each channel. The number of coupons tested was largely dependent on the width of each segment. The material properties of mild steel gusset plates of 6mm and 8mm thicknesses (used in ECT-2) were evaluated from six tensile coupon tests. Three coupons were cut from the 6mm thick gusset plates and another three from the 8mm thick gusset plates. The coupons were prepared and tested in a 100 kN Instron machine, according to the guidelines provided by the British Standard, BS EN ISO 6892-1 [10]. The average yield stress (f_y), ultimate stress (f_u), modulus of elasticity (E) of the channels and gusset plates, and the average dimensions of the channels, are presented in Table 1.

Longitudinal web coupons (LWC) and longitudinal flange coupons (LFC) were tested in order to use their average ultimate stress and average yield stress to calculate the bearing resistance and moment of resistance of the channels, respectively. This is because webs largely resist bearing forces and flanges largely resist bending moments in connections. Longitudinal corner

coupons (LCC) were tested in order to ensure that LFC did not inherit the properties of LCC, especially in channels with narrow flanges. The average material properties of the LFC of the 300x50x20x3 channel significantly inherited the properties of LCC; hence results of LWC were adopted throughout the investigation, as a conservative approach. The Young's modulus of elasticity (E) of each channel was derived from averaging the slope of the stress-strain curve of the web coupons over the elastic region.

Table 1. Average material properties and dimensions of the channels and gusset plates

Channel section	Specimen	f_y (MPa)	f_u (MPa)	E (GPa)	H (mm)	w (mm)	d (mm)	t (mm)
$300 \times 75 \times 20 \times 3$	LWC	240.828	321.256	207	300.05	75.00	20.00	3.01
	LFC	253.900	331.654					
	LCC	366.885	406.089					
$300 \times 65 \times 20 \times 3$	LWC	228.666	309.215	206	300.02	65.01	20.00	3.00
	LFC	240.330	317.852					
	LCC	322.244	375.391					
$300 \times 50 \times 20 \times 3$	LWC	255.153	335.048	208	300.00	50.00	20.01	3.00
	LFC	330.550	367.675					
	LCC	379.962	402.319					
6 mm gusset plate	LC	342.754	463.619	201				
8 mm gusset plate	LC	351.865	496.859	200				

Size M20, grade 8.8 high strength structural steel bolts were selected for the connections. These bolts are manufactured according to SANS 1700 [11]. A shear strength calculation showed that the selected bolts are adequate for all the connections. Material tests on the bolts were not done since the strength of the bolts ($f_{ub} \geq 800$ MPa) is less critical than the bearing strength of cold-formed steel channels and hot-rolled steel gusset plates used. A 2 mm bolt-hole clearance was adopted to reduce large slips in the connections and standard steel washers were placed on both sides of the bolt to prevent excessive rotation of the bolt.

3.0 Model of the test frames

To simplify the experimental work, a model was developed to represent, as much as possible, the behaviour of the region around the internal eaves connection of a double-bay portal frame structure. This is illustrated by the circled part, ABC, of the complete double-bay portal frame, shown in Figure 6. Points B and C are the points of contraflexure in the rafters and point A is the point of contraflexure in the column. Boundary conditions of the extracted portion of the eaves connection were modelled to simulate the actual boundary conditions in a full double-bay portal frame. Testing of a full double-bay portal frame structure was avoided because of the cost and the limited space in the laboratory.
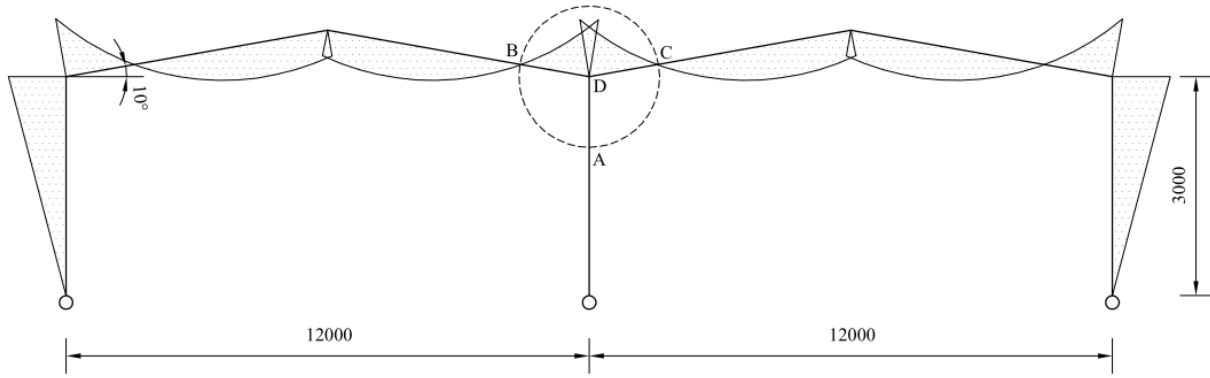
Figure 6: Double-bay portal frame subjected to vertical downward loading.

A total of nine different frames were tested (three with ECT-1 connections and six ECT-2 connections), with variables given in Table 2. These variables include the width of the channel flanges, strength of the channels, number of bolts, connection configuration and thickness of the hot-rolled gusset plate. The depth, thickness and the size of the lip of the channels were not varied. In Table 2, parameters t_g, f_{yg}, f_{yc}, L_r, H_c, t_g and e represent the thickness of the gusset plate, yield strength of the gusset plate, yield strength of the channel, eaves-to-contraflexure length of the rafters, eaves-to-contraflexure height of the column and the lever arm, respectively. To validate the results of each frame, two frames with the same variables were tested.

Table 2: Variables in the test frames

Frame	Channel Section	t_g (mm)	f_{yg} (MPa)	f_{yc} (MPa)	L_r (m)	H_c (m)	Bolts	(e) m
ECT-1.1	300x75x20x3.0	N/A	N/A	240.828	2.00	1.00	8, M20	1.08
ECT-1.2	300x65x20x3.0	N/A	N/A	228.666	2.00	1.00	8, M20	1.08
ECT-1.3	300x50x20x3.0	N/A	N/A	255.153	2.00	1.00	8, M20	1.08
ECT-2.1	300x75x20x3.0	6 mm	342.754	240.828	1.70	0.70	12, M20	1.12
ECT-2.2	300x65x20x3.0	6 mm	342.754	228.666	1.70	0.70	12, M20	1.12
ECT-2.3	300x50x20x3.0	6 mm	342.754	255.153	1.70	0.70	12, M20	1.12
ECT-2.4	300x75x20x3.0	8 mm	351.865	240.828	1.70	0.70	12, M20	1.12
ECT-2.5	300x65x20x3.0	8 mm	351.865	228.666	1.70	0.70	12, M20	1.12
ECT-2.6	300x50x20x3.0	8 mm	351.865	255.153	1.70	0.70	12, M20	1.12

4.0 Test Frame, instrumentation and test procedure

A portal frame resist bending, shear and axial loads when subjected to vertical downward loading. To induce these forces, two forces (P) were applied simultaneously to the frames ECT-1 and ECT-2, as shown in the schematic diagrams in Figs. 7 and 8. Photographs of the actual test set-up are shown in Figs. 9 and 10. In ECT-1 frames, two rafters were connected to the column, back-to-back, with one rafter connected to the column at a lower level than the other. Points A and D are the load application points in the lower rafter (LR) and upper rafter (UR), respectively, while points E and F are the load application points in the in the column. Points B and C represents the lower rafter-to-column and upper rafter-to-column joints, respectively. Point G is the base of the column. The lever arm (e) is the perpendicular distance from the upper rafter-to-column and lower rafter-to-column connections to the applied load (P).

As for ECT-2 frames, the two cold-formed rafters were connected, back-to-back, to the cold-formed column, at the same level through a hot-rolled gusset plate. ECT-2 has three joints namely; the gusset plate-to-column joint (J), the left rafter-to-gusset plate joint (I) and the right

7

rafter-to-gusset plate joint (K). Points H and L are the load application points in the left and right rafters, respectively. Point M is the load application point in the column for both rafters and point N is the column base. Similarly to ECT-1, the lever arm (e) represents the perpendicular distance from the gusset plate-to-column joint to the applied load (P). In both ECT-1 and ECT-2, the column and rafters were connected back-to-back at the eaves connection to counterbalance the eccentricities of the connected channels, thus resisting lateral buckling of the channels [2, 3, 4].
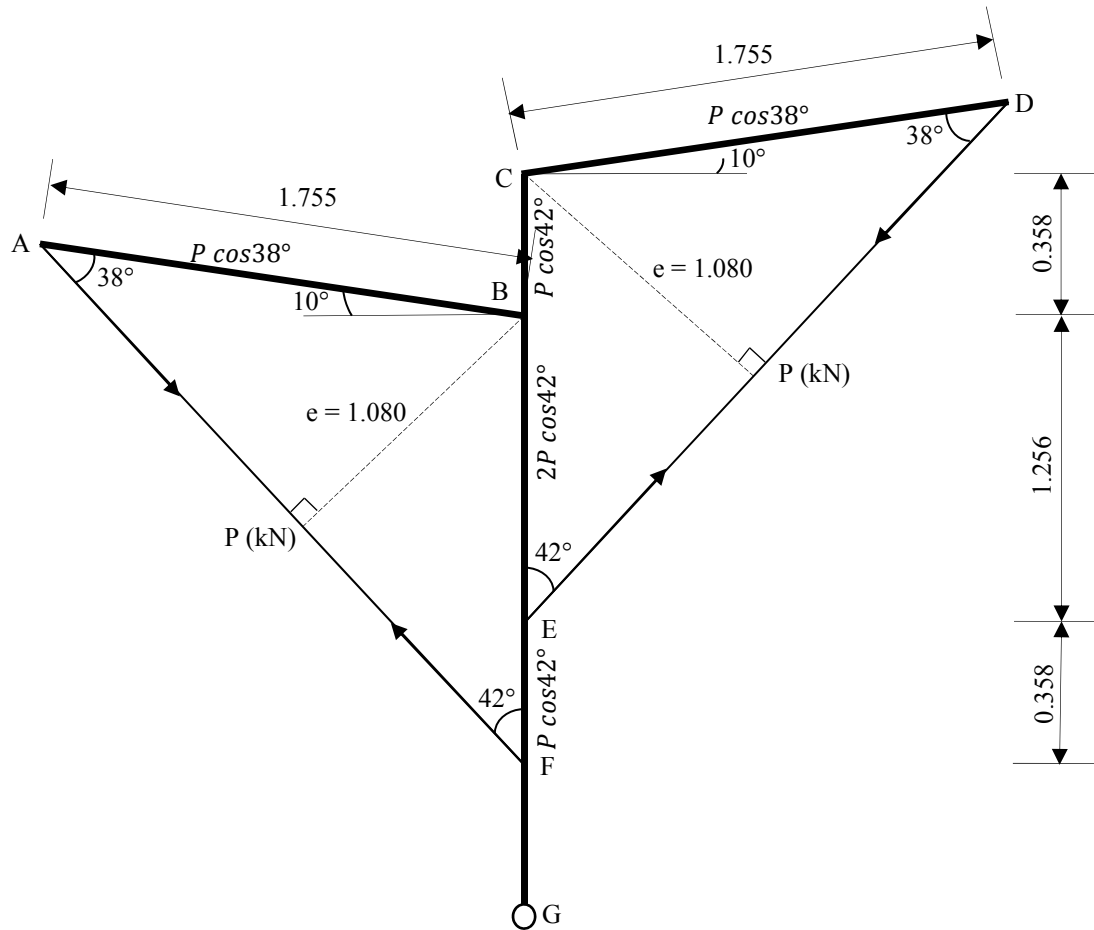

Figure 7: Layout and geometry of ECT-1 test set-up

Figure 8: Layout and geometry of ECT-2 test set-up

The test frames were assembled on the laboratory floor and lifted onto a 1.52m testing platform using a crane. The testing platform was mounted onto the laboratory floor in order to raise the height of the column and accommodate the hydraulic cylinders and load cells, as illustrated in Figure 9 and 10. Three mild steel angle cleats (one for the column web and two for the column flanges) were welded on top of the cap plate of the testing platform to provide the base connection for the column. Since the investigation focused on the capacity and performance of the central eaves joint, the rafters were restrained with 2, 3 m high columns, spaced at 130 mm apart, to eliminate possible lateral-torsional buckling of the rafters, which could distort the test results. To facilitate a smooth movement between the webs of the rafters and the restraining columns, three alwayse ball transfer units were incorporated into the restraints. Two diagonal bracings were welded from the central columns to the outer columns (rafter restraints) to increase the stability and rigidity of the restraining columns. The height of the columns was reduced to eliminate lateral-torsional buckling of the column during testing.

The rotations at the eaves joint were measured using rotation transducers, which were installed at the centre of each joint. Rotation transducers were mounted vertically at the centre of each joint inside both rafters. Curvature of the rafter, just outside the joints, was measured using two strain gauges. Before testing, all the test instruments and software were checked to ensure that they are working properly. The loads were applied in line with the shear centre of the rafters to minimise twisting, using 2, 10 tonne hydraulic jacks. Both rafters were subjected to simultaneous equal loads, using flat bars, to simulate the actual loading conditions of the portal frame. Load increments of 0.5 kN at two minute intervals were applied up to ninety percent of the expected failure load, thereafter the loading interval was increased to three minutes. This was done to observe the failure modes of the frames. Rotations and strain data were recorded using a data logger, and applied loads were recorded by means of two load cells. Visual observations were made and recorded during testing. After each test was done, the frame was dismantled and bolt-hole elongations physically measured and recorded.

Figure 9: Typical test set-up of ECT-1 frames

Figure 10: Typical test set-up of ECT-2 frames

5.0 Failure mechanism

Two failure mechanisms were observed in the frames, viz; local buckling in the compression zone of the web and flange of the channels, and bearing distortion of bolt-holes. Local buckling was the eventual failure mode in all the nine frames. In ECT-1 frames, local buckling started in the compression web of the column, between the top and bottom connections, followed by local buckling of the compression flange (see Figure 11). Local buckling, between the top and bottom connections, is attributed to the unbalanced in-plane moment in the column, caused by staggering the eaves connections. Figure 12 shows the bending moment diagram of the extracted portion of the ECT-1.1 frame, to illustrate the unbalanced moment in the column. This portion of the column is susceptible to local buckling failure since the web of the column is not stiffened, unlike in the connections, where the web of the column is stiffened by the web of the rafter.

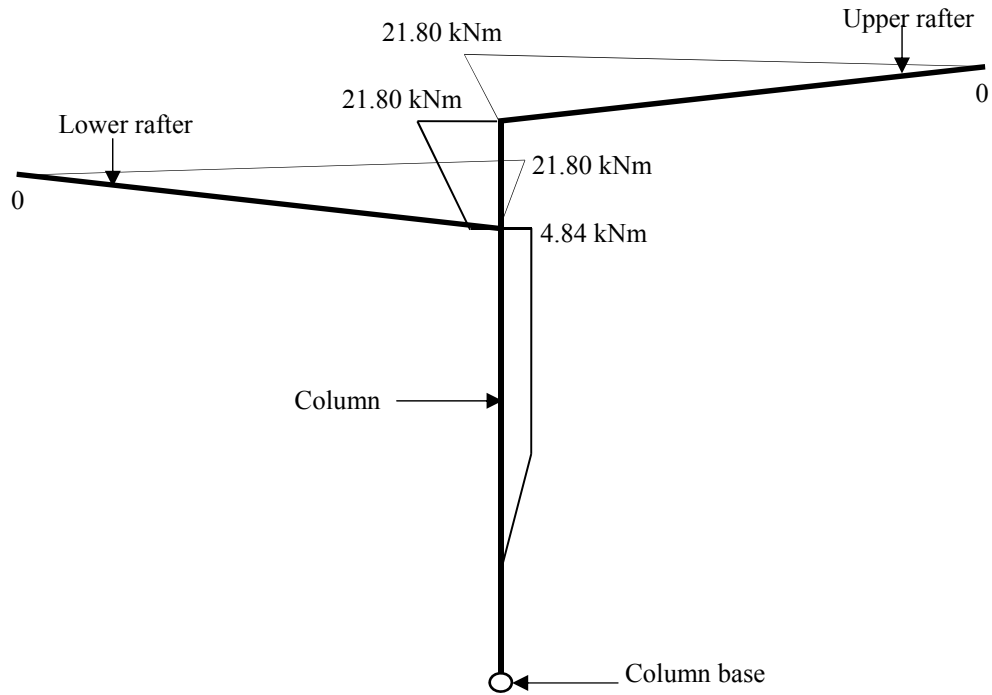Figure 11: Local buckling failure in ECT-1 frames

Figure 12: Bending moment diagram of ECT-1.1 frame

In ECT-2 frames, local buckling took place in the web of both rafters first, just outside the rafter-to-gusset plate connection, followed by local buckling of the compression flange. Local buckling occurred after substantial rotation of the rafters. Typical local buckling failure of ECT-2 frames is shown in Figure 13. Since the moments in the rafters (Figure 14) balance at the eaves joint of these frames, there was no moment at the joint, and the column resisted an axial compression load force only. A small amount of lateral deflection was observed in both the frames with the 6mm gusset plates, during testing.

Although both ECT-1 and ECT-2 frames failed by local buckling of the web and flange of the channel section, there was also considerable bolt-hole distortions observed after disassembling the frames. The size of the bolt-hole elongations ranged from 1.5 mm to 2.5 mm, and elongated in the direction of the bolt force due to the moments. This proves that the bolt forces due to moments contribute more to the resultant bolt forces, compared to bolt forces due to axial and shear forces.
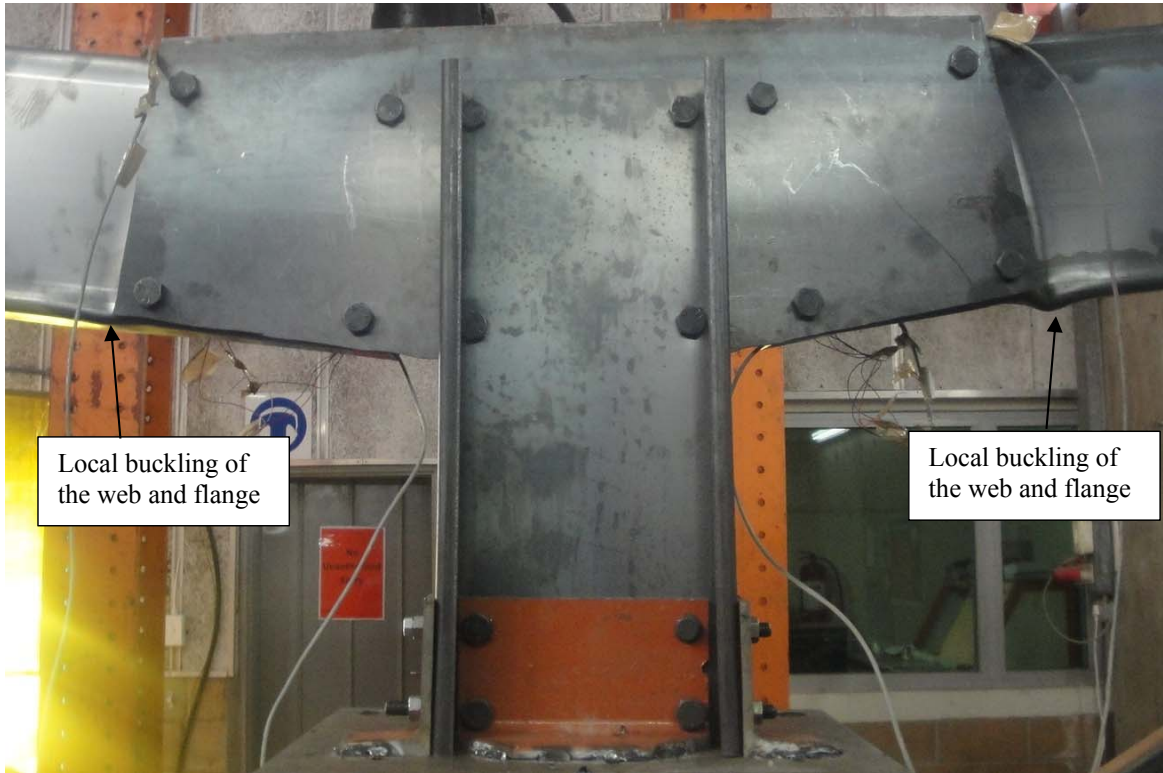
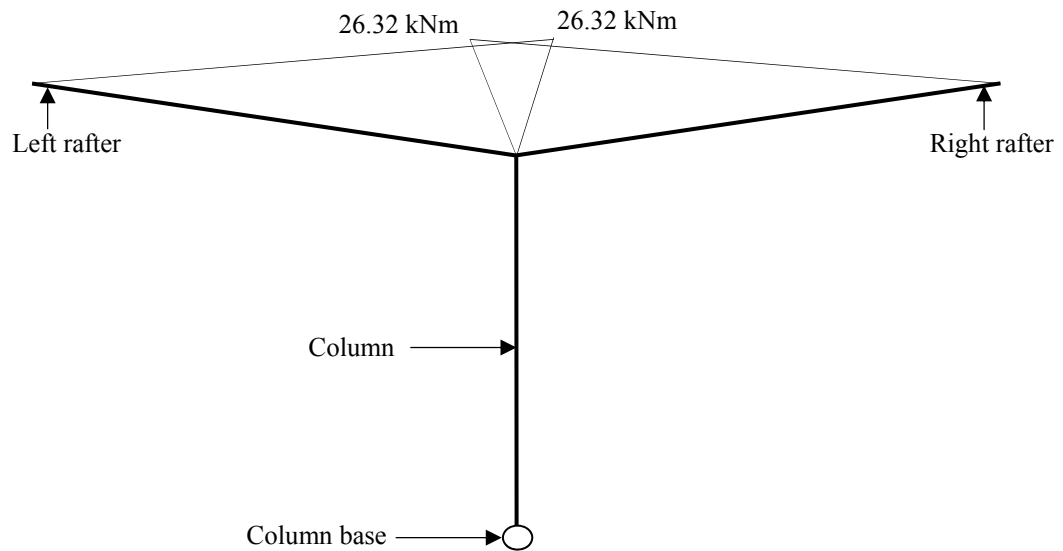Figure 13: Local buckling failure in ECT-2 frames

Figure 14: Balanced column moments in ECT-2.1 frame

6.0 Experimental and theoretical results

A summary of the maximum applied loads (P) and the resulting maximum joint first-order moments (M_{ex}), axial (N_R in the rafter and N_C in the column) and shear forces (V_R in the rafter and V_C in the column) obtained from the experiments is shown in Table 3. The eaves joint moments (M_{ex}) are calculated from the product of the applied load (P) and the initial eccentricity (e). The moments (M_{ex}) at the rafter-gusset plate connection are determined using

proportion, since the bending moment diagrams in the rafters are linear. The maximum moments achieved by the frames were influenced by the flange width and yield strength of the channels. Frames formed from channels with larger flange width and higher yield strength achieved larger bending moments and vice versa. In ECT-1, frames ECT-1.1 and ECT-1.2 were expected to achieve larger moments than frame ECT-1.3 because of the larger flange width, however this did happen because frame ECT-1.3 had higher yield strength than frames ECT-1.1 and ECT-1.2. ECT-2 frames with 6 mm thick mild-steel gusset plates produced lower experimental moments of resistance compared to frames with 8 mm thick mild-steel gusset plates. The lower moment capacities in the connections with 6mm thick gusset plates, versus the 8mm thick gusset plates, were probably a result of the small lateral deflection, caused by the smaller stiffness of the 6mm gusset plate.

Table 3: Applied loads, moments, axial and shear forces

Frame	Section	f_y (MPa)	t_g (mm)	P (kN)	e (m)	M_{ex} (kNm)	N (kN)		V (kN)	
							N_R	N_C	V_R	V_C
ECT-1.1	300×75×20×3	240.83	N/A	20.18	1.08	21.80	15.90	29.99	12.42	13.50
ECT-1.2	300×65×20×3	228.67	N/A	19.05	1.08	20.57	15.01	28.31	11.73	12.75
ECT-1.3	300×50×20×3	255.15	N/A	21.02	1.08	22.70	16.56	31.24	12.94	14.07
ECT-2.1	300×75×20×3	240.83	6 mm	23.50	1.12	21.42	18.52	34.93	14.47	0.00
ECT-2.2	300×65×20×3	228.67	6 mm	23.30	1.12	21.23	18.36	34.63	14.34	0.00
ECT-2.3	300×50×20×3	255.15	6 mm	21.41	1.12	19.51	16.87	31.82	13.18	0.00
ECT-2.4	300×75×20×3	240.83	8 mm	27.25	1.12	24.83	21.47	40.50	16.78	0.00
ECT-2.5	300×65×20×3	228.67	8 mm	25.29	1.12	23.05	19.93	37.59	15.57	0.00
ECT-2.6	300×50×20×3	255.15	8 mm	23.73	1.12	21.63	18.70	35.27	14.61	0.00

To validate the experimental results, the code-predicted calculations were performed. The cross-sectional moment and shear resistance of the hot-rolled steel gusset plates and cold-formed channel sections were calculated, based on the Canadian steel standard (CAN/CSA-S16-09 [12]) and the North American Standard (AISI S100: 2013 [13]), respectively. Table 4 summarises the code-predicted resistances of the cold-formed channel sections and hot-rolled steel gusset plates. The yield moment ($M_y = Z_{ef}f_y$), axial load ($N_y = A_{ef}f_y$) and shear resistance ($V_r = A_w f_v$) of the cold-formed channels are calculated based on the effective cross-sectional properties of the channels, where Z_{ef} is the effective section modulus, A_{ef} is the effective cross-section area, f_y is the yield stress of the web and f_v is the limiting shear stress. As for the hot-rolled steel gusset plates, the moment and shear resistance were computed from $M_{rg} = Z_e f_y$ and $V_{rg} = 066A f_y$, respectively, where Z_e is the elastic section modulus, A is the cross sectional area and t_g is the thickness of the gusset plate.

Table 4: Yield resistances of cold-formed steel sections and hot-rolled steel gusset plates

Frames	Sections	Hot-rolled gusset plates				Cold-formed channels			
		f_y (MPa)	t_g (mm)	M_{rg} (kNm)	V_{rg} (kN)	f_y (MPa)	M_y (kNm)	N_y (kN)	V_r (kN)
ECT-1.1	300×75×20×3.0	N/A	N/A	N/A	N/A	240.83	28.15	236.48	94.13
ECT-1.2	300×65×20×3.0	N/A	N/A	N/A	N/A	228.67	24.72	212.84	91.50
ECT-1.3	300×50×20×3.0	N/A	N/A	N/A	N/A	255.15	24.09	209.79	95.10
ECT-2.1	300×75×20×3.0	342.75	6.0	45.79	496.10	240.83	28.15	236.48	94.13
ECT-2.2	300×65×20×3.0	342.75	6.0	45.79	496.10	228.67	24.72	212.84	91.50
ECT-2.3	300×50×20×3.0	342.75	6.0	45.79	496.10	255.15	24.09	209.79	95.10
ECT-2.4	300×75×20×3.0	351.87	8.0	62.67	679.04	240.83	28.15	236.48	94.13
ECT-2.5	300×65×20×3.0	351.87	8.0	62.67	679.04	228.67	24.72	212.84	91.50
ECT-2.6	300×50×20×3.0	351.87	8.0	62.67	679.04	255.15	24.09	209.79	95.10

A comparison of yield resistances of the channels and applied experiment results, in Table 5, shows the theoretical yield moment (M_y), axial compressive resistance (N_y) and shear resistance (V_r) of the channels to be greater than the experimental moment (M_{ex}), axial forces (N_{max}) and shear forces (V_{max}) of the joint. This means that all the frames failed to reach the unfactored yield moment, axial and shear resistance of the connected members, because of local buckling. The moment capacity of the frames ECT-1.1, ECT-1.2 and ECT-1.3 achieved 77%, 83% and 94% of the yield capacity of the connected members, respectively. ECT-2 connections formed from 6 mm thick gusset plates achieved between 76% and 86% of the moment capacity of the connected members while those formed from 8 mm thick gusset plates achieved between 88% and 93% of the moment capacity of the connected members. As indicated above, the lower moment capacities in the connections with 6mm thick gusset plates, versus the 8mm thick gusset plates, were probably a result of the small lateral deflection, caused by the smaller stiffness of the 6mm gusset plate.

Table 5: Comparison of yield strengths of the channels and experimental results

Frame	Section	f_y (MPa)	Yield strengths			Experiment results				
			M_y (kNm)	N_y (kN)	V_r (kN)	M_{ex} (kNm)	N_{max} (kN)	V_{max} (kN)	e_x (mm)	B (kNm²)
ECT-1.1	300×75×20×3.0	240.83	28.15	236.48	94.13	21.80	29.99	13.50	28.0	0.61
ECT-1.2	300×65×20×3.0	228.67	24.72	212.84	91.50	20.57	28.31	12.75	23.5	0.48
ECT-1.3	300×50×20×3.0	255.15	24.09	209.79	95.10	22.70	31.24	14.07	16.8	0.38
ECT-2.1	300×75×20×3.0	240.83	28.15	236.48	94.13	21.42	34.93	14.47	28.0	0.60
ECT-2.2	300×65×20×3.0	228.67	24.72	212.84	91.50	21.23	34.63	14.34	23.5	0.50
ECT-2.3	300×50×20×3.0	255.15	24.09	209.79	95.10	19.51	31.82	13.18	16.8	0.33
ECT-2.4	300×75×20×3.0	240.83	28.15	236.48	94.13	24.83	40.50	16.78	28.0	0.70
ECT-2.5	300×65×20×3.0	228.67	24.72	212.84	91.50	23.05	37.59	15.57	23.5	0.54
ECT-2.6	300×50×20×3.0	255.15	24.09	209.79	95.10	21.63	35.27	14.61	16.8	0.36

Local buckling seems to have initiated at the flange-web joint due to the combined influence of in-plane bending moment and bimoment stresses [14]. A bimoment (B) is defined as the product of the in-plane or major axis moment (M_{ex}) and the eccentricity of the web centerline from the shear center (e_x). The background of this concept is well established in [1, 15, 16, 17]. The bimoment bends each flange about its own (horizontal) plane, inducing compression stresses at the bottom flange/web junction and tension stresses at the bottom flange/lip junction. When a channel section is subjected to negative in-plane or major axis moment, the bottom flange is in compression, which is the case in the inside flange of the connections in Figures 11 and 13. The effect of the bimoment is to increase the major axis compression stresses at the bottom flange/web junction, whilst at the same time reducing the compression stresses at the bottom flange/lip junction. The stress distribution of this combined effect is shown in Figure 15, where compression is negative and tension is positive. Due to the combined stresses, an increased compression stress is expected in the bottom half of the web and the inside part of the bottom flange. Effectively this relieves the bottom flange from distortional buckling, but reduces the local buckling critical stress in the web.
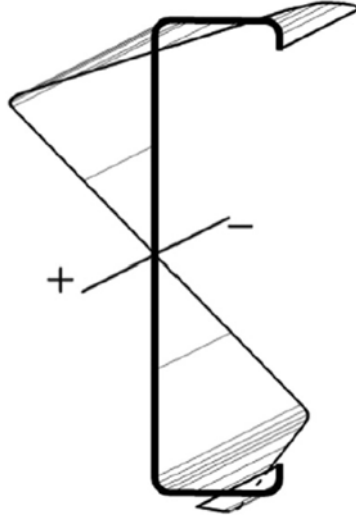
Figure 15 Stress distribution due to combined in-plane bending and bimoment [14]

In all the tested structures, the connections did not fail. This suggests that the connections were not the critical part in these tests. In order to relate the capacity of the connections to the capacity of the frames, the theoretical moment of resistance of the connections (M_{rj}), was computed using the bearing resistance (B_r) of the channels, since this is more critical than the shearing resistance of the bolts (V_{rb}). The bearing resistance (B_r) of the connections and the shearing resistance of the bolts (V_{rb}) are determined from Equation 1 and 2 [12], respectively.

$$B_r = atf_u \leq Cdtf_u \qquad (1)$$

$$V_{rb} = 0.70 \times 0.60 nmA_b f_{ub} \qquad (2)$$

where, a is the distance from the centre of the hole to the edge of the connected element, in the direction of the force, t is the thickness of channel, d is the diameter of the bolt, f_u is the minimum tensile strength of the channel, C is the bearing coefficient, A_b is the cross-sectional area of bolt, n is the number of bolts, m is the number of faying surfaces or shear planes in a bolted joint and f_{ub} is the is tensile strength of the bolt. Kemp [18] proposed that the bearing coefficient of thin plates with threaded bolts be C = 1.8. In the shearing resistance equation of the bolts, the factor 0.6 converts the tensile stress into a shear stress, while 0.70 is used if the bolt threads are intercepted by the shear plane.

A comparison of the experimental results and the theoretical moment of resistance of the connections (M_{rj}) is given in Table 6. Note that the bolts in the gusset-to-rafter connections are subjected to equal axial, shear forces and moments, because the joint is symmetrical. It is clear from this table that the connections were not critical in most frames. Most members failed to achieve a moment capacity equal to that of the connections. This agrees with the test results since failure occurred in the channels, and not in the connection. In ECT-1 frames, the ratio of maximum moment (M_{ex}) to the theoretical moment of resistance of the joints (M_{rj}) varied from 0.94 to 0.95. Provided that the channels are of the same material properties, channels with wider flanges resist larger moments than those with smaller flanges. However, ECT-1.3 exhibited the largest maximum moment (M_{ex}), despite having the smallest flange channel (50 mm). This is attributed to the high material strength of the 300x50x20x3 channel.

16

Although the ratio of the maximum moment (M_{ex}) to the theoretical moment of resistance of the connections (M_{rj}) of connections ECT-2.1 and ECT-2.2 suggest that the connections were more critical, this was not the case. A ratio of M_{ex} to M_{rj} of almost 1 implies that the joints were just about to fail when the rafters failed by local buckling. Despite the fact that the gusset plates were not critical, frames fabricated from 8mm gusset plates produced higher ratios of M_{ex} to M_{rj} compared to those formed from 6mm gusset plates. This was probably caused by the small lateral deflection experienced by the 6mm gusset plates.

From the analysis above it seems that the material properties of the cold-formed channels influenced the ultimate moments more than the width of the cold-formed steel channel flanges in ECT-1 frames. However, this was not the case in ECT-2 frames. In ECT-2 frames, the width of the cold-formed steel channel flanges and the thickness of the hot-rolled gusset plates influenced the ultimate moments more than the material properties of the cold-formed channels. Except frame ECT-2.1, all frames fabricated from the 300x75x20x3 channel sections in this group produced the highest ultimate moments, followed by the 300x65x20x3 channel sections, and the least ultimate moments were produced by the 300x50x20x3 channel sections. It should also be noted that although the yield resistance of the channels is larger than the moment of resistance of the connections, the channels did not fail by yielding, but local buckling.

Table 6: Experimental and theoretical moment of resistance of the connections

Frame	Section	M_{ex} (kNm)	M_y (kNm)	f_u (MPa)	V_r (kN)	B_r (kN)	M_{rj} (kNm)	$\dfrac{M_{ex}}{M_{rj}}$
ECT-1.1	300×75×20×3.0	21.80	28.15	321.26	105.56	34.70	22.85	0.95
ECT-1.2	300×65×20×3.0	20.57	24.72	309.22	105.56	33.40	22.00	0.94
ECT-1.3	300×50×20×3.0	22.70	24.09	335.05	105.56	36.19	23.83	0.95
ECT-2.1	300×75×20×3.0	21.42	28.15	321.26	105.56	34.70	22.57	0.95
ECT-2.2	300×65×20×3.0	21.23	24.72	309.22	105.56	33.40	21.72	0.98
ECT-2.3	300×50×20×3.0	19.51	24.09	335.05	105.56	36.19	23.54	0.83
ECT-2.4	300×75×20×3.0	24.83	28.15	321.26	105.56	34.70	22.57	1.10
ECT-2.5	300×65×20×3.0	23.05	24.72	309.22	105.56	33.40	21.72	1.06
ECT-2.6	300×50×20×3.0	21.63	24.09	335.05	105.56	36.19	23.54	0.92

Moment-Rotation and Curvature Curves

Moment-rotation curves and moment-curvature curves are used to explain the behaviour of the connections and rafters, just outside the connection, respectively. A summary of the maximum average applied moments (M_{ex}), rotation (ϕ), curvature (κ) and secant rotational stiffness of the joint (K) of the tested frames is shown in Table 7. It should be noted that the maximum moments, rotations, curvatures and joint rotational stiffness are the maximum values at frame failure and not at joint failure since the joint did not fail in all the frames tested. Figure 16 shows the moment-rotation curves of the upper rafter (UR) and lower rafter (LR) of ECT-1 frames, and Figure 17 shows the moment-rotation curves of ECT-2 frames. Each moment-rotation curve represents the average curve for the two connections of the tested frame. Non-smooth graphs were caused by the jacking process of the frames as the load was applied to the frames.

The moment-rotation curves for all the tested structures show negligible rotation at the initial loading stage as the load was resisted by friction, between the connected members. Thereafter, the moment-rotation relationships curves are linear up to load levels close to ultimate moment. After this phase, the response of the connections became non-linear due to bearing distortions

in the bolt holes. In all connections tested ECT-2 connections generated much less rotation than ECT-1 connections. The maximum rotations produced by ECT-1 connections, of $0.032 - 0.033$ rad, show useful ductility.

The average secant rotational stiffness of the joints were obtained from dividing the maximum moment (M_{ex}) by the respective maximum rotation (ϕ), excluding the friction phase of the moment-rotation curves. Table 7 and the graphs in Figure 16 and 17 show that ECT-2 connections are stiffer and less ductile than ECT-1 connections. The average elastic joint rotational stiffnesses (ϕ_{sj}) of ECT-1 connections ranges from $660 - 688$ kNm/radian, and are significantly lower than the stiffnesses of ECT-2 connections with 6mm gusset plates, which ranges from $1179.44 - 1338.75$ kNm/radian. Among all the frames tested, connections with 8mm gusset plates attained the largest stiffnesses of $1773.08 - 2403.33$ kNm/radian. This large difference in stiffness is attributed to the material properties and thickness of the gusset plates used.

Table 7: Summary of average rotation, stiffness and curvature results

| Frame	Channel Section	t_g (mm)	f_{yg} (MPa)	f_{yc} (MPa)	M_{ex} (kNm)	ϕ (rad)	K (kNm/rad)	κ (1/mm) 10^{-6}
ECT-1.1	300x75x20x3.0	N/A	N/A	240.828	21.80	0.033	660.61	10.41
ECT-1.2	300x65x20x3.0	N/A	N/A	228.666	20.57	0.032	642.81	7.16
ECT-1.3	300x50x20x3.0	N/A	N/A	255.153	22.70	0.033	687.88	5.28
ECT-2.1	300x75x20x3.0	6.0	342.754	240.828	21.42	0.016	1338.75	6.35
ECT-2.2	300x65x20x3.0	6.0	342.754	228.666	21.23	0.018	1179.44	6.26
ECT-2.3	300x50x20x3.0	6.0	342.754	255.153	19.51	0.015	1300.67	6.18
ECT-2.4	300x75x20x3.0	8.0	351.865	240.828	24.83	0.012	2069.17	7.67
ECT-2.5	300x65x20x3.0	8.0	351.865	228.666	23.05	0.013	1773.08	6.52
ECT-2.6	300x50x20x3.0	8.0	351.865	255.153	21.63	0.009	2403.33	6.33
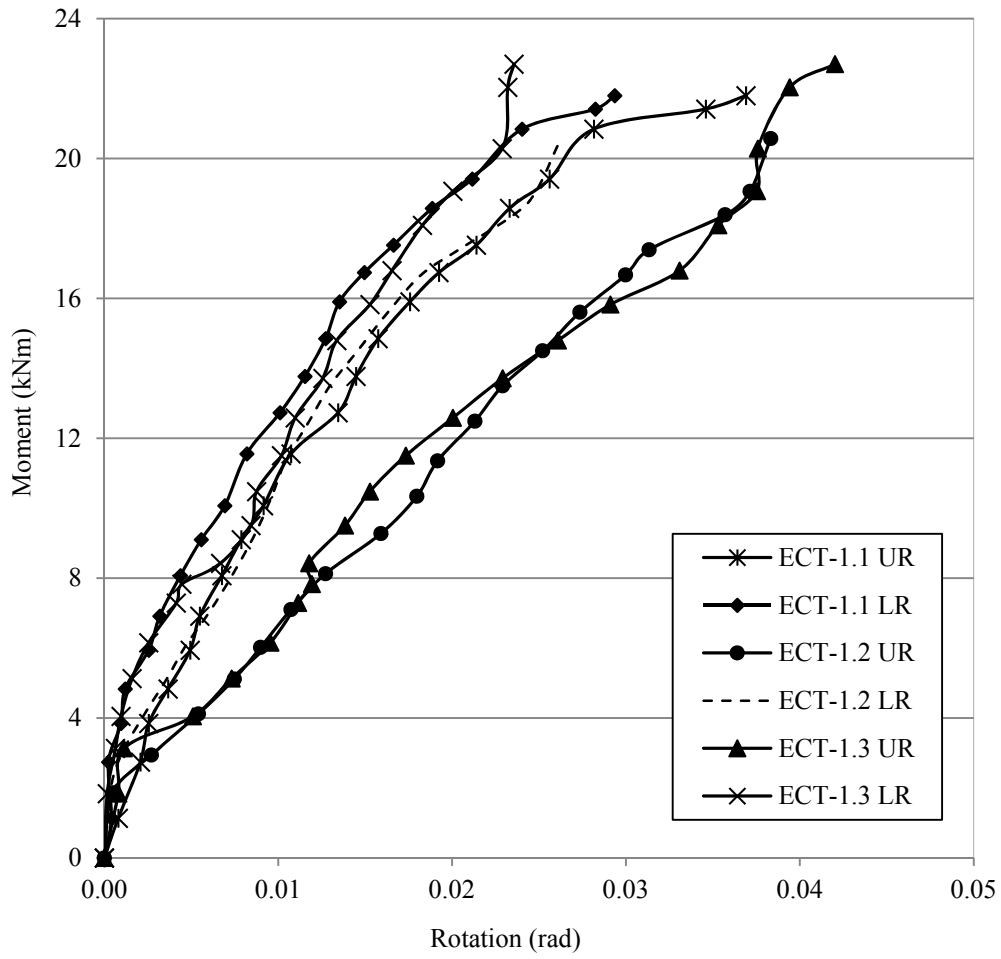
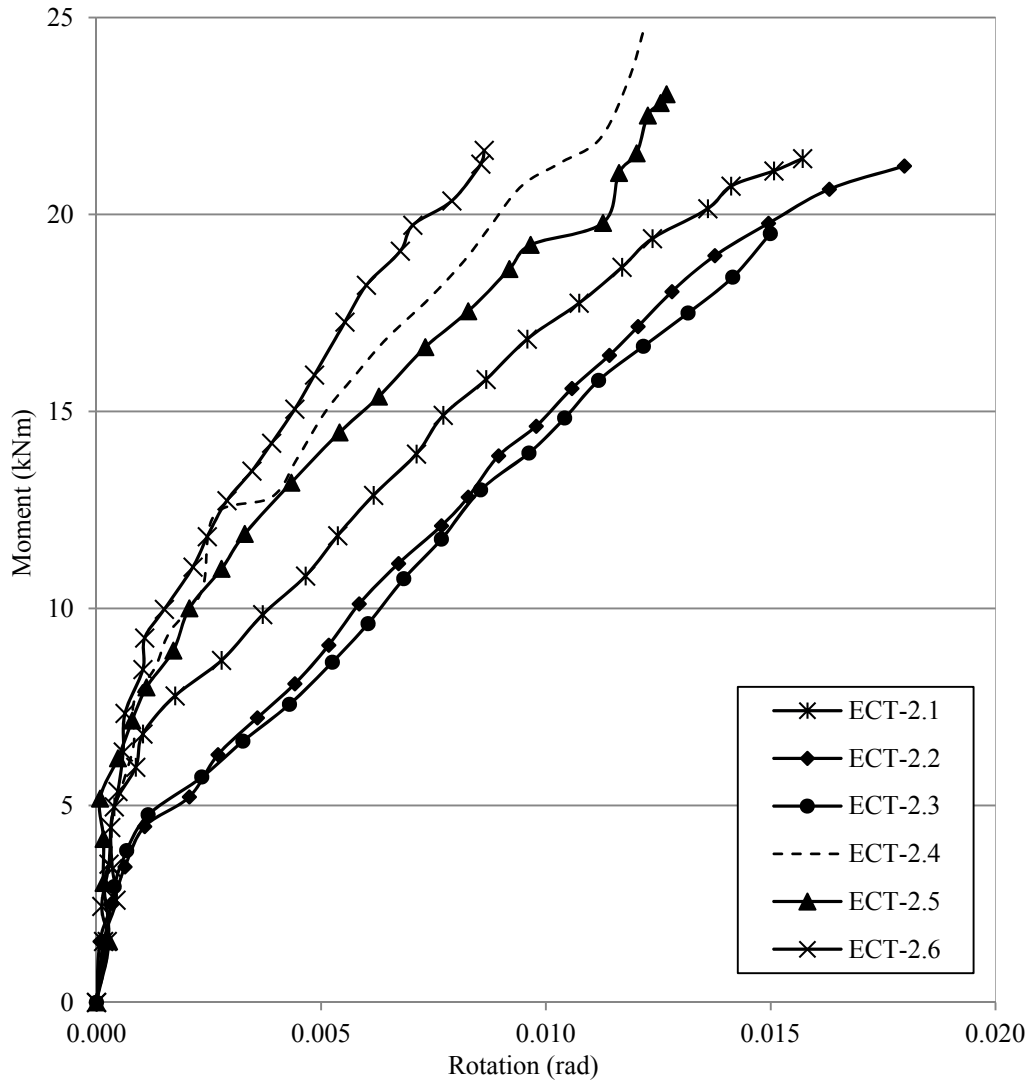Figure 16: Moment-rotation curves of ECT-1 connections

Figure 17: Moment-rotation curves of ECT-2 connections

The curvature (κ) was computed from the strain readings at the top and bottom flanges of the channels, immediately after the connection, since this is the section where the maximum strain was expected. The moment-curvature curves for ECT-1 and ECT-2 frames are shown in Figures 18 and 19, respectively. Similarly to moment-rotation curves, each moment-curvature curve represents the average curve for the tested frame of each type. Also, as for moment-rotation curves, the moment-curvature curves for ECT-1 and ECT-2 are largely linear-elastic. The moment-curvature curves became non-linear towards the maximum load of the frames. Curvatures for frames with gusset plates varied by a small margin, viz; curvatures for ECT-2 frames with 6 mm thick mild-steel gusset plates ranged from 6.18×10^{-6} to 6.35×10^{-6} mm^{-1}, while curvatures for ECT-2 frames with 8 mm thick mild-steel gusset plates ranged from 6.33×10^{-6} to 7.67×10^{-6} mm^{-1}. In both cases, curvatures tend to decrease with a decrease in flange width.
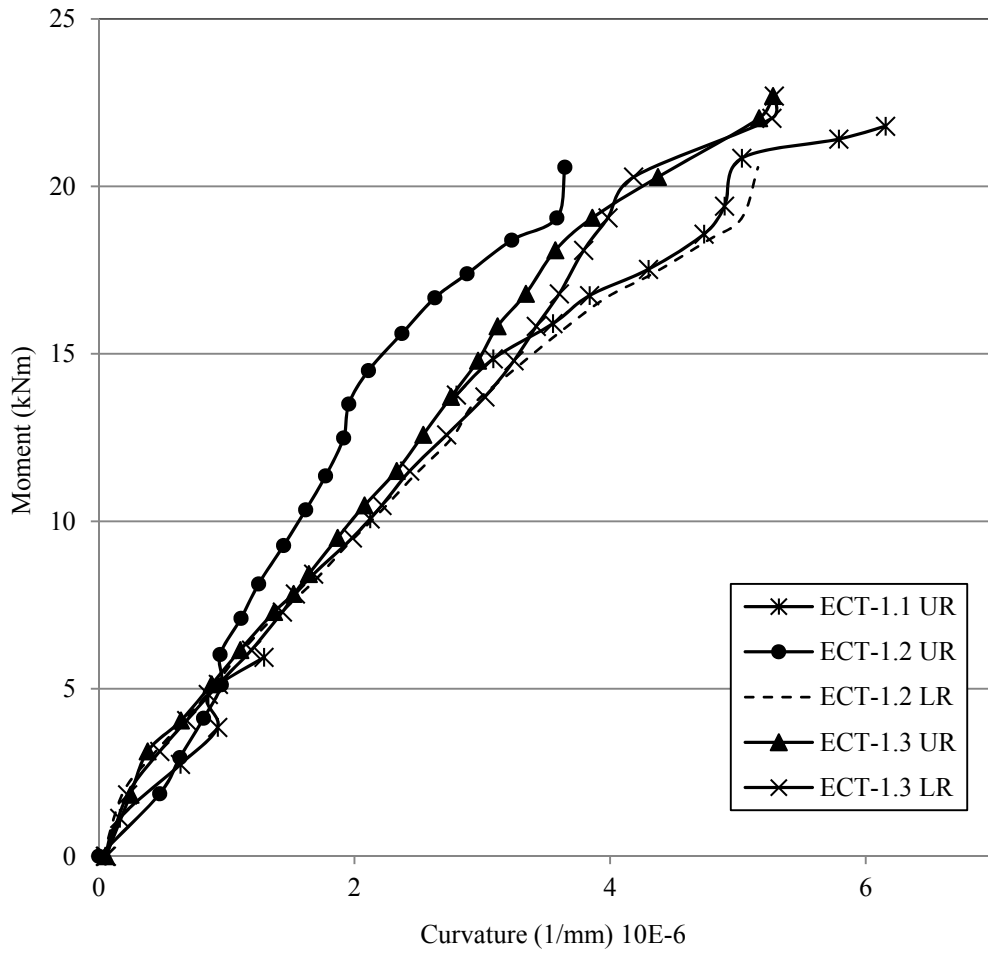
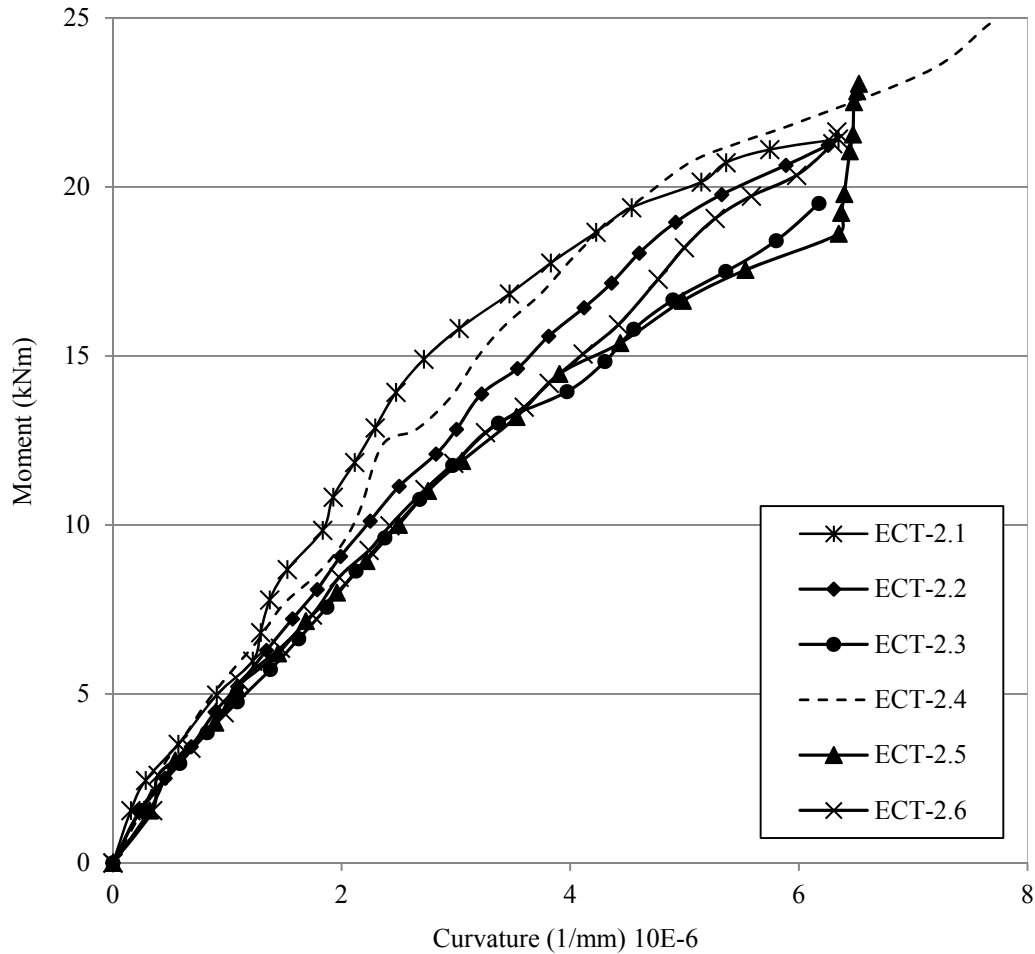Figure 18: Moment-curvature curves of ECT-1 frames

Figure 19: Moment-curvature curves of ECT-2 frames

8.0 Conclusions

This research has presented two different configurations of connecting single channel cold-formed rafters used in double-bay portal frame frames, namely; ECT-1 (with staggered single channel cold-formed rafters) and ECT-2 (gusseted rafter-to-column connections). ECT-1 connections joints utilise fewer bolts (8 M20 bolts), does not make use of a secondary elements like a gusset plate, hence the material and labour costs are expected to be significantly less compared to ECT-2 frames, which utilises 12 M20 bolts and a gusset plate.

Tests conducted on these connections demonstrated that the connections were not critical. This explains the reason why the capacities of the frames is almost the same. Although all frames failed by local buckling, the position of failure varied from one connection type to the other. In ECT-1, local buckling started in the web of the column between the staggered connections, followed immediately by local buckling of the flange. Local buckling, between the top and bottom connections, is attributed to the unbalanced moment in the column, caused by staggering the eaves connections. In ECT-2, local buckling failure started in the web of both rafters, just outside the connections, followed by local buckling of the flange. The moments in the rafters are balanced at the eaves joint of these frames, implying that there was no moment at the joint, and the column resisted an axial compression force only. In both frames, local

buckling seems to have started at the flange-web joint due to the combined influence of in-plane bending moment and a bimoment, resulting from non-uniform torsion or in-plane bending moment applied in a plane of the thin-walled section eccentric from the shear centre.

Although significant bolt-bearing deformations around bolt-holes were observed in all cold-formed channels of the tested frames, no bearing failure was observed. The distortions were influenced more by the larger forces due to moment than by the resultant of the axial and shear forces. Minor gusset plate deflections were observed in ECT-2 frames towards joint failure, and might have caused a small loss of moments in the frames with 6mm gusset plates. Increasing the gusset plate thickness from 6 to 8mm in ECT-2 frames did not change the critical moment of resistance of the frames. This is because failure of the frames were in the channels, with the same material properties and section size.

References

[1]   Baigent AH, Hancock GJ. The Behaviour of Portal Frames Composed of Cold-Formed Members. Thin-Walled Frames - Recent technical advances and Trends in Design, Research and Construction, Oxford, Elsevier Applied Science 1982; 209-222.

[2]   Dundu M. The use of cold-rolled channels in light, small-span portal frames using back-to-back bolted connections in bearing. PhD Thesis, School of Civil and Environmental Engineering, University of the Witwatersrand 2003.

[3]   Dundu M, Kemp AR. Strength requirements of single cold-formed channels connected back-to-back. Journal of Constructional Steel Research 2006a;62:250-261.

[4]   Dundu M, Kemp AR. Plastic and lateral-torsional buckling behaviour of single cold-formed channels connected back-to-back. Journal of Structural Engineering 2006b; 132(8) ASCE, 132, 8 (2006) 1223-1233.

[5]   Dundu M. Design approach of cold-formed steel portal frames. International Journal of Steel Structures, Korean Soc. Steel Construction (KSSC) 2011; 11(3):259-273.

[6]   Dundu M. Base Connections of Single Cold-Formed Steel Portal Frames, Journal of Constructional Steel Research 2012;78:38-44.

[7]   Bukasa G, Dundu M. Use of angle cleats to restrain cold-formed channels against lateral torsional instability. Journal of Constructional Steel Research 2016; 123:144–153.

[8]   Tshuma B, Dundu M. Eaves connections of double-bay portal frames with staggered single channel cold-formed rafters, The Sixth International Conference on Structural Engineering, Mechanics and Computation (SEMC), 5-7 September 2016, Cape Town.

[9]   Tshuma B, Dundu M. Gusseted rafter-to-column connections of double-bay single channel portal frames, The Sixth International Conference on Structural Engineering, Mechanics and Computation (SEMC), 5-7 September 2016, Cape Town.

[10]   BS EN ISO 6892-1. Tensile testing of metallic materials: Part 1 - Method of test at room temperature. British Standard Institution; 2009.

[11]   SANS 1700. South Africa standard for the manufacture of fasteners. South African Bureau of Standards, Pretoria; 2004.

[12]   CAN/CSA-S16-09. Limit states design of steel frames. Canadian Standards Association, Rexdale, Ontario, Canada; 2009.

[13]   AISI S100. 2013. North American specification for the design of cold-formed steel structural members. Washington D.C: AISI; 2013.

[14]   Lim JBP, Hancock GJ, Clifton GC, Pham CH, Das R. DSM for ultimate strength of bolted moment-connections between cold-formed steel channel members. Journal of Constructional Steel Research 2016;117:196–203

[15] Baigent AH, Hancock GJ. Structural analysis of assemblages of thin-walled members. Engineering Structures 1982;4(3):207-216

[16] Vlasov V. Thin-walled elastic beams. Israel Program for Scientific Translations, Jerusalem, Israel, 1961.

[17] Zbirohowski-Koscia K. Thin walled beams: From theory to practice, Crosby Lockwood, 1967.

[18] Kemp AR. Bearing capacities and modes of failure in single-bolt lap joints. Journal of the South African Institution of Civil Engineering 2001;43(1): 13-18.